Journal of Inflammation Research

Dovepress
open access to scientific and medical research

Open Access Full Text Article

ORIGINAL RESEARCH

Identification and Analysis of PANoptosis-Related Genes in Sepsis-Induced Lung Injury by Bioinformatics and Experimental Verification

Zhen Yang[1,*], Xingyu Kao[1,*], Na Huang[1], Kang Yuan[2], Jingli Chen[2], Mingfeng He[2]

[1]The Eighth School of Clinical Medicine, Guangzhou University of Chinese Medicine, Foshan, Guangdong Province, People's Republic of China; [2]Foshan Hospital of Traditional Chinese Medicine, Foshan, Guangdong Province, People's Republic of China

*These authors contributed equally to this work

Correspondence: Jingli Chen; Mingfeng He, Email fstcmcjl@126.com; he-mingfeng@foxmail.com

Purpose: Sepsis-induced lung injury (SLI) is a serious complication of sepsis. PANoptosis, a novel form of inflammatory programmed cell death that is not yet to be fully investigated in SLI. Our research aims to screen and validate the signature genes of PANoptosis in SLI by bioinformatics and in vivo experiment.

Methods: SLI-related datasets were downloaded from NCBI Gene Expression Omnibus (GEO) database. Differentially expressed genes (DEGs) of SLI were identified and intersected with the PANoptosis gene set to obtain DEGs related to PANoptosis (SPAN_DEGs). Then, Protein–Protein Interaction (PPI) network and functional enrichment analysis were conducted based on SPAN_DEGs. SVM-REF, LASSO and RandomForest three algorithms were combined to identify the signature genes. The Nomogram and ROC curves were performed to predict diagnostic value. Immune infiltration analysis, correlation analysis and differential expression analysis were used to explore the immunological characterization, correlation and expression levels of the signature genes. Finally, H&E staining and qRT-PCR were conducted for further verification in vivo experiment.

Results: Twenty-four SPAN_DEGs were identified by intersecting 675 DEGs with the 277 PANoptosis genes. Four signature genes (CD14, GSDMD, IL1β, and FAS) were identified by three machine learning algorithms, which were highly expressed in the SLI group, and had high diagnostic value in the diagnostic model. Moreover, immune infiltration analysis showed that most immune cells and immune-related functions were higher in the SLI group than those in the control group and were closely associated with the signature genes. Finally, it was confirmed that the cecum ligation and puncture (CLP) group mice showed significant pathological damage in lung tissues, and the mRNA expression levels of CD14, IL1β, and FAS were significantly higher than the sham group.

Conclusion: CD14, FAS, and IL1β may be the signature genes in PANoptosis to drive the progression of SLI and involved in regulating immune processes.

Keywords: sepsis, lung injury, PANoptosis, machine learning, immune infiltration analysis

Introduction

Sepsis is a common life-threatening systemic inflammatory disease caused primarily by a dysregulated response to pathogenic infection.[1] Multiple organs may be damaged during the development of sepsis, the lung is especially vulnerable, occurs the earliest and is one of the most common organs to fail.[2] Approximately 50% of patients with sepsis develop acute lung injury (ALI).[3] Additionally, sepsis is also the dominant cause of acute respiratory distress syndrome (ARDS) or ALI. The main pathological signatures of ARDS/ALI are acute inflammation, alveolar epithelial injury, interstitial edema and immune cell infiltration.[4] Few efficient drugs or therapies are available to treat sepsis-induced lung injury (SLI) at present, resulting in a higher mortality rate and poor prognosis as well.[5] Anti-inflammatory therapy, noninvasive ventilation, invasive mechanical ventilation, extracorporeal membrane oxygenation and supportive

Received: 30 November 2023
Accepted: 20 February 2024
Published: 28 March 2024

care are the main treatments in clinical.[6] However, the exact molecular mechanisms of SLI remain unclear, and the development of new and effective therapeutic strategies is urgently needed.

Cell death has been proven to play a crucial role in infections, inflammatory diseases, neurodegenerative diseases, cancer, etc. With the continuous updating of cell death modalities such as apoptosis, pyroptosis, autophagy, ferroptosis, and cuproptosis, recent studies have uncovered complex cross-linking process between cell death patterns.[7] PANoptosis ("P" for pyroptosis, "A" for apoptosis, and "N" for necroptosis) is an inflammatory programmed cell death regulated by the PANoptosome complex, with key signatures of pyroptosis, apoptosis and necroptosis.[7] Some biomarkers related to PANoptosis, including TNF receptor 1 (TNFR1), cysteinyl aspartate-specific proteinase (caspase)-3, caspase-7 and caspase-8 for apoptosis, NOD-like receptor thermal protein domain associated protein 3 (NLRP3), apoptosis-associated speck-like protein containing a CARD (ASC), caspase-1, and Gasdermin D (GSDMD) for pyroptosis, TNFR1, receptor-interacting protein kinase 1 (RIPK1), RIPK3, caspase-8, and mixed-lineage kinase domain-like (MLKL) for necroptosis have shown a fairly strong link in inflammatory disease pathogenesis.[8] The organism participates in PANoptosis by regulating the activation and inhibition of cell death during bacterial infection mainly through TLRs and related death receptor (including TRIF, FADD, MyD88, and RIPK1) through alters activation status, gene expression, and protein localization of cell death initiator proteins.[9] Previous studies have revealed that MiR-29a-3p could ameliorate ALI by reducing the level of inflammatory factors and downregulate PANoptosis-related genes Z-DNA binding protein 1 (ZBP1), GSDMD, caspase-3, caspase-8, and MLKL in mice lung tissues.[10] Besides, pyroptotic macrophages can release danger-associated molecular pattern molecules and danger signals to enhance the inflammatory response during the pathogenesis of sepsis-associated ALI.[11] Moreover, it was demonstrated that the macrophage-excretive exosome Aminopeptidase N (APN) could trigger lung epithelial cell necroptosis through APN-related mechanisms in SLI.[12,13] Consequently, different types of programmed cell death are involved in inflammatory responses and tissue damage, and play an important role in maintaining tissue homeostasis in SLI. It would be sensible to infer that PANoptosis may be closely associated with the pathological mechanism of SLI.

However, the role of PANoptosis in SLI remains unclear, and requires further exploration. Bioinformatics and machine learning have emerged as potential strategies for exploring underlying mechanisms and potential biomarkers.[14] In the study, R tool and the limma package were used to perform differential gene analysis based on the four data sets, and then merged differentially expressed genes (DEGs) with PANoptosis genes to obtain DEGs related to PANoptosis (SPAN_DEGs) for functional enrichment analysis. The signature genes were identified by three machine learning algorithms, including support vector machine-recursive signature elimination (SVM-RFE), least absolute shrinkage and selection operator (LASSO) logistic regression, and RandomForest (RF). Subsequently, the Nomogram and receiver operating characteristic (ROC) curves were established for diagnostic value prediction. Immune infiltration analysis and the signature genes correlation with infiltrating immune cells were performed to investigate the mechanisms of immunity in SLI. Then, gene correlation analysis and differential expression analysis were implemented to explore the correlation and expression levels of the signature genes. Finally, we verified the results by hematoxylin and eosin (H&E) staining and quantitative real-time PCR (qRT-PCR) in animal experiments. In summary, the research can provide new therapeutic targets for sepsis patients with lung injury.

Materials and Methods

Data Acquisition and Preprocessing

Sequencing data of GSE15379, GSE23767, GSE52474 and GSE60088 from mice lung tissues were downloaded from the NCBI Gene Expression Omnibus[15] (GEO; https://www.ncbi.nlm.nih.gov/geo/). The specific information of these datasets is displayed in Table 1. The raw datasets were pre-processed by "affy" in R, each probe name in microarray datasets was converted into corresponding gene symbol. Then, these datasets were normalized, the average value was taken as its expression value when multiple probes corresponded to a common gene. Batch effects and other unwanted variance between the two datasets were eliminated using the surrogate variable analysis (SVA) package from Bioconductor. Subsequently, the SLI-related genes expression matrix file was identified for the following analysis. The LIMMA package with p-value <0.05 and |log2 fold-change (FC)|≧0.5 as screening criteria was applied to screen DEGs between

Table 1 The Summarized Information of Microarray Datasets

GEO Data Set	Platform	Control	SLI
GSE15379	GPL1261	3	3
GSE23767	GPL6887	3	8
GSE52474	GPL1261	15	10
GSE60088	GPL1261	4	5

the control and SLI groups. The expression heat maps and Volcano plot of the DEGs were presented by using the R package pheatmap and ggplot2. Meanwhile, 277 PANoptosis-related genes were identified from the published literature by merging the gene lists of apoptosis, necroptosis and pyroptosis while removing redundant genes.[16] Finally, DEGs were intersected with PANoptosis-related genes to obtain SPAN_DEGs.

Construction of PPI Network and Functional Enrichment Analysis

To explore the correlations between SPAN_DEGs, the SPAN_DEGs gene set was imported into STRING website (version 12.0, https://string-db.org/) to construct PPI (protein–protein interaction) network. The TSV file was downloaded and then imported to the cytoscape 3.7.0 for visualization, the size of the nodes and the thickness of the connecting lines were plotted according to the degree and combined score. Gene ontology (GO) and Kyoto Encyclopedia of Genes and Genomes (KEGG) enrichment analyses were performed to investigate the biological functions and related signaling pathways of SPAN_DEGs. Go consists of cellular components (CC), molecular functions (MF) and biological pathways (BP) and is used to analyze gene function and biological processes.[17] KEGG is now widely used to explain the functions and involved pathways of genes. Furthermore, we used subset sets from the Molecular Signatures Database for Gene Set Enrichment Analysis (GSEA) to assess the pertinent pathways and molecular mechanisms based on phenotypic categorization and gene expression profiles.[18]

Acquisition of the Signature Genes by Machine Learning Algorithms

Three machine learning algorithms, including SVM-RFE, LASSO logistic regression analysis, and RF algorithm, were utilized to screen the signature genes from SPAN_DEGs. SVM-REF is a machine learning method based on support vector machines, which finds the best variables by censoring the signature vectors generated by SVM.[19] LASSO logistic regression identifies variables mainly by finding the λ with the smallest classification error by "glmnet" package and is mainly used to screen signature variables to construct the best classification model.[20] SPAN_DEGs were ranked by using the RF algorithm, and the relative value above 0.25 was considered to be typical of chance causes.[21] Finally, the genes obtained by intersecting the three machine learning algorithms with each other were regarded as the signature genes.

Construct a Diagnostic Nomogram and ROC Analysis

We used the "rms" R package to create a nomogram to predict the recurrence of SLI by adding the score corresponding to each factor and transferring the overall score to the bottom scale.[22,23] ROC curves were visualized to present the area under the curve (AUC) for evaluating their diagnostic value. In general, an AUC of 0.5 indicates no discrimination, whereas values between 0.7 and 0.8 are regarded as acceptable, between 0.8 and 0.9 as excellent, and beyond 0.9 is considered outstanding.[24]

Immune Infiltration Analysis

The immune infiltration analysis was investigated using ssGSEA based on immunologic signature gene sets, which contained two parts: 16 immune cell types (activated dendritic cells (aDCs), B cells, CD8+ T cells, DCs, immature DCs (iDCs), macrophages, mast cells, neutrophils, natural killer (NK) cells, plasmacytoid DCs (pDCs), T helper cells, T follicular helper (Tfh), T helper type 1 (Th1) cells, Th2 cells, tumor-infiltrating lymphocytes (TIL), regulatory T (Treg)) and 13 immune function types (antigen presenting cell (APC) co-inhibition, APC co-stimulation, chemokine

C-C-Motif receptor (CCR), check-point, cytolytic_activity, human leukocyte antigen (HLA), inflammation promoting, major histocompatibility complex (MHC) class I, parainflammation, T-cell co-inhibition, T-cell co-stimulation, type I interferon (IFN) response, Type II IFN response). The various levels of infiltration of immune cells and immune function types between the control group and the SLI group were performed. Besides, we analyzed the correlation between the signature genes and immune cells and immune function types based on Spearman correlation analysis.

Correlation Analysis and Difference Analysis of the Signature Genes

To investigate the correlation between the signature genes, the "corrplot" package was used to perform correlation analysis between the signature genes. Meanwhile, the expression levels of the signature genes in the control and SLI groups were implemented by using "ggpubr" package.

Animal Modeling and Animal Group

6–8-weeks old male C57BL/6 mice, weighting 20–22 g, were purchased from Guangzhou Regal Biotechnology Co., Ltd. (SCXK (Yue) 2021-0059, Guangzhou, China). All mice were housed in a standard specific pathogen-free (SPF) level laboratory animal room with a standard at 22–24 °C and 50–60% relative humidity with 12/12–h light/dark schedule.

SLI model was established by cecum ligation and puncture (CLP) method as previously published protocol.[25] Adaptive feeding for 3 days, all mice were fasted for 12 h before operation and drinking freely. Mice were anesthetized by intraperitoneal injection of 1% pentobarbital (0.08 mL/10 g), the peritoneum was then opened to 1–2 cm to expose the cecum. We ligated the distal point of the ileocecal valve of the cecum with a 4–0 silk ligature and punctured it twice with a 21G needle, then gently squeezed a small amount of feces before returning the cecum to its original position in the abdominal cavity and closing it. The mice in the sham group were simply exposed to the cecum by laparotomy and then closed without CLP. After operation, all mice were subcutaneously injected with 0.9% normal saline (37°C, 0.5mL/10g) and rewarmed until resuscitation. After 24 h of surgery, all mice were sacrificed and collected lung tissue.

Histopathologic Analysis

Fresh lung tissue was fixed with 4% paraformaldehyde (PFA) for at least 24 h, dehydrated with gradient ethanol, paraffin embedded, sectioned into 4 μm slices for hematoxylin and eosin (H&E), and observed lung pathological injuries under the optical microscope. Histopathologic scoring criteria of lung injury consists of five areas, namely neutrophil infiltration, alveolar congestion, interstitial edema, alveolar hemorrhage and thickening of the alveolar wall, each item was scored 0–3, from no injury to severe injury.[26]

RNA Extraction and Quantitative Real-Time PCR (qRT-PCR)

We used qRT-PCR to verify the differential expression of mRNAs for the characterized genes. Total RNA of lung tissue was extracted by using Trizol reagent (Invitrogen, Carlsbad, CA, USA), the purity and concentration of total RNA was detected using a MicroplateReader (BioTek Epoch 2, Vermont, USA). According to the cDNA synthesis kit (RR037A, Takara, Japan), the mRNA was reverse-transcribed into complementary DNA (cDNA) (Applied Biosystems™ 2720 Thermal Cycler, Thermo Fisher Scientific, Waltham, MA, USA). The mRNA expression levels were measured with the SYBR® Premix Ex Taq™ II (RR820A, Takara, Japan) by using Applied Biosystems® 7500 Fast Real-Time PCR System (Applied Biosystems Inc., Carlsbad, CA, USA). Relative mRNA levels were calculated using the $2^{-\Delta\Delta}$CT method. The primer sequences used in the experiments were synthesized by Shanghai Shenggong Technology Co., Ltd, which are presented in Table 2.

Statistical Analysis

R software (v.4.1.0) and GraphPad Prism 9.5.0 (GraphPad Software, San Diego, CA, USA) were used for statistical analysis and figures construction. Continuous variables were displayed as mean±standard deviation (SD), Student's *t*-test or Wilcoxon test was employed to compare whether there is a significant difference between the two groups of data. $P < 0.05$ indicated statistical significance.

Table 2 Primers Used for qRT-PCR

Gene Name	Forward Primer	Reverse Primer
CD14	CTCTGTCCTTAAAGCGGCTTAC	GTTGCGGAGGTTCAAGATGTT
FAS	TATCAAGGAGGCCCATTTTGC	TGTTTCCACTTCTAAACCATGCT
GSDMD	CCATCGGCCTTTGAGAAAGTG	ACACATGAATAACGGGGTTTCC
IL-1β	GAAATGCCACCTTTTGACAGTG	TGGATGCTCTCATCAGGACAG
β-actin	GTGACGTTGACATCCGTAAAGA	GCCGGACTCATCGTACTCC

Abbreviations: qRT-PCR, quantitative real-time PCR; CD14, cluster of differentiation 14; FAS, factor-related Apoptosis; GSDMD, Gasdermin D; IL-1β, Interleukin—1β.

Results

Identification of SPAN_DEGs and Functional Enrichment Analysis

The merged GEO datasets contained 25 control group samples and 26 SLI group samples, these samples were normalized and presented in a box plot (Figure 1A). Under the criteria of p-value <0.05 and |log2FC| ≧ 0.5, 675 DEGs were identified, with 465 up-regulated genes and 210 down-regulated genes. The volcano plot, a heat map as well as box plots of typical DEGs visually showed the results of differential expression analysis (Figure 1B–D). The PANoptosis gene set was composed of 27 genes related to pyroptosis, 259 genes related to apoptosis, 15 genes related to necrosis (Figure 1D, Supplementary Table 1). We mapped 675 DEGs and PANoptosis gene set to obtain 24 common genes, defined as PANoptosis-associated DEGs for SLI (SPAN_DEGs) (Figure 2A).

We constructed PPI network to explore the interrelationships between SPAN_DEGs, a total of 24 nodes and 118 edges in the PPI network (Figure 2B). To further investigate the importance of these genes, a node's size and color depend on its degree, the tightness of the connection between the nodes is indicated combined score (Figure 2C). The top 15 GO terms were shown in a bubble chart (Figure 2D). BP enrichment revealed SPAN_DEGs are mainly enriched in apoptotic process, positive regulation of nuclear factor kappa B (NF-κB) transcription factor activity, positive regulation of DNA-binding transcription factor activity, positive regulation of cytokine production, positive regulation of IL-8 production. Enriched CC is related to membrane raft, death-inducing signaling complex, endosome membrane, cytoplasmic vesicle membrane, caveola. MF enrichment revealed SPAN_DEGs are mainly enriched in tumor necrosis factor receptor superfamily binding, death receptor binding, endopeptidase activity, protein serine/threonine kinase activity, caspase recruitment domain (CARD) domain binding. KEGG enrichment analysis suggested that SPAN_DEGs were mainly enriched in TNF signaling pathway, NOD-like receptor signaling pathway, cytosolic DNA-sensing pathway, Toll-like receptor signaling pathway, NF-kappa B signaling pathway (Figure 2E). The results of GSEA analysis showed that SPAN_DEGs were mainly involved in IL-17 signaling pathway, NOD-like receptor signaling pathway (Figure 2F). Overall, these results showed that NOD-like receptor signaling pathway, TNF signaling pathway were the main pathways, suggesting they may be involved in inflammatory response and oxidative stress.

Selection of the Signature Genes

A total of 5 predicted signature genes (CD14, GSDMD, DYNLL1, PSMD9, and STAT3) were obtained by SVM-RFE machine learning algorithm (Figure 3A). Seven predicted signature (CD14, IL1β, TNF, IRF1, GSDMD, SNAI2, and FAS) genes were selected from statistically significant variables by LASSO regression analysis (Figure 3B). The top 10 genes with relative importance (CD14, CASP4, IL1β, FAS, MYD88, GSDMD, BID, STAT3, and IRF1) were screened by RF algorithm (Figure 3C and D), the specific results are presented in Table 3. Finally, we used a Venn diagram to show that the four signature genes (CD14, GSDMD, IL1β, and FAS) that overlapped each other were found through the intersection of the three machine learning algorithms described above (Figure 3E).

Construction and Evaluation of a Diagnostic Nomogram

We constructed a diagnostic nomogram for the signature genes (CD14, GSDMD, IL1β, and FAS) using the rms package (Figure 4A) and assessed their predictive efficacy employing calibration curves. The result of calibration curves showed

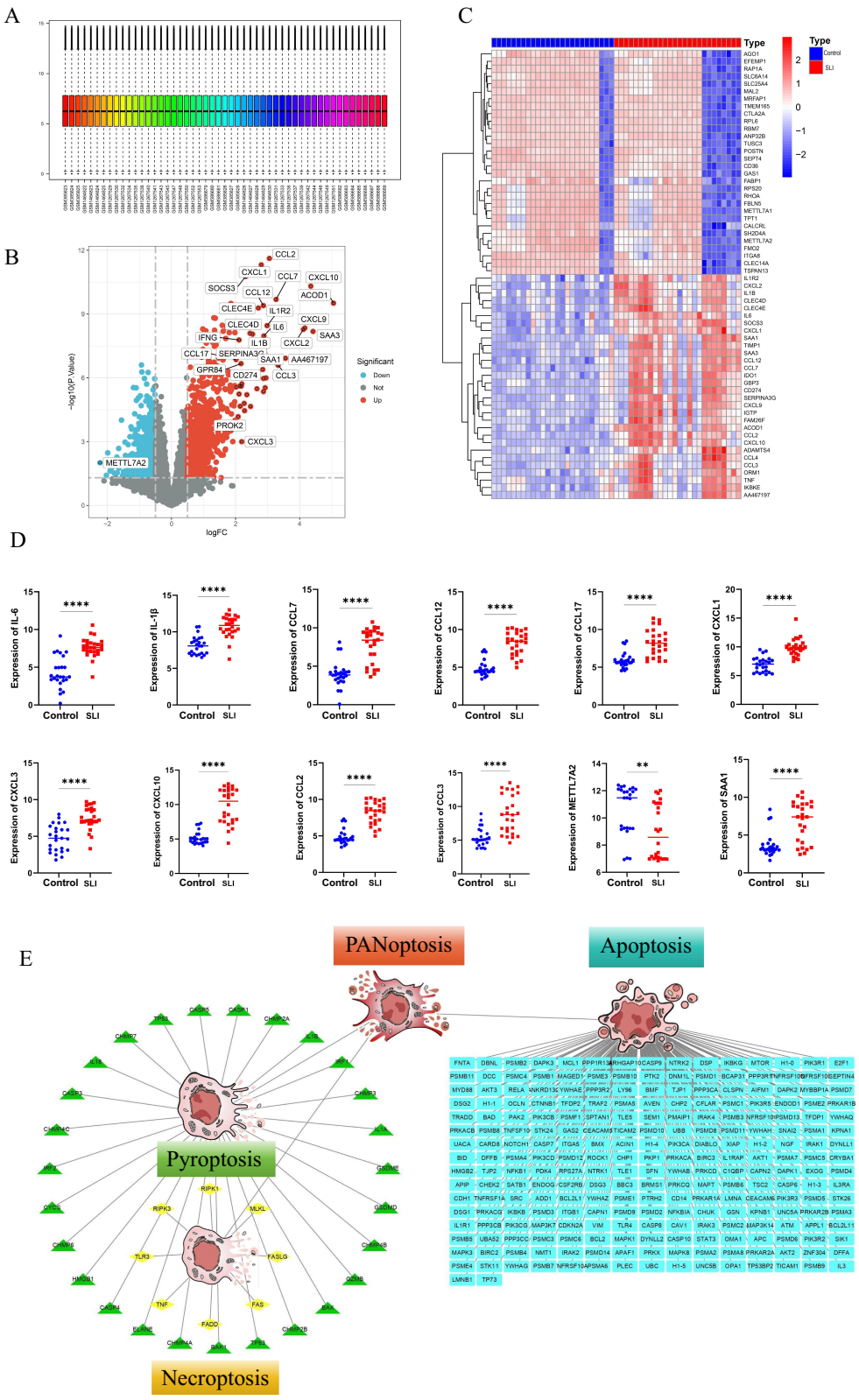

Figure 1 Data preprocessing and differential gene analysis. (**A**) Boxplot after normalization of raw data between samples. (**B**) Volcano plot of DEGs. Red represents up-regulated DEGs, grey represents no significant difference, and blue represents down-regulated DEGs. (**C**) Heat map of DEGs. Red indicates theDEGs is highly expressed in the sample, and blue indicates the DEGs is lowly expressed in the sample. (**D**) Box plots of typical DEGs. (**E**) The PANoptosis gene list. **p < 0.01, ****p < 0.0001.

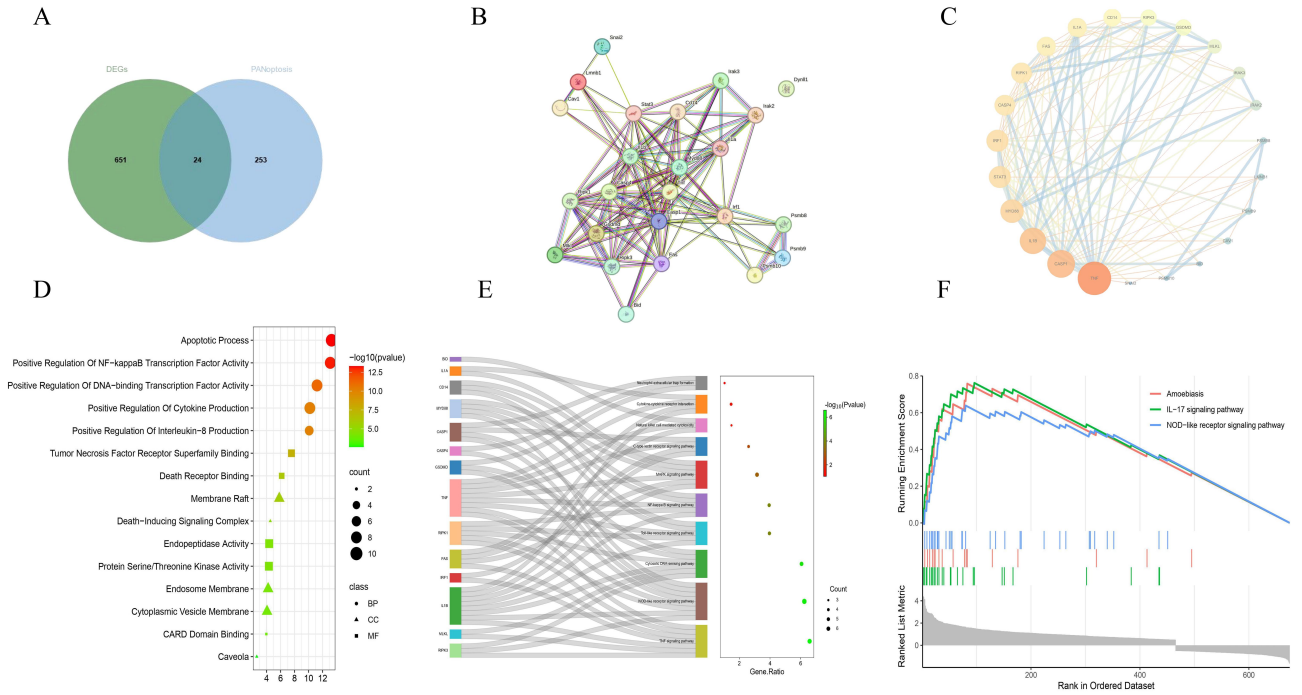

Figure 2 PPI network construction and functional analysis of SPAN_DEGs. (**A**) The Venn diagram of DEGs versus PANoptosis related genes. (**B**) PPI network of SPAN_DEGs. (**C**) The core target network of SPAN_DEGs. (**D**) GO analysis based on the SPAN_DEGs. (**E**) KEGG enrichment analysis based on the SPAN_DEGs. (**F**) GSEA analysis based on the SPAN_DEGs.

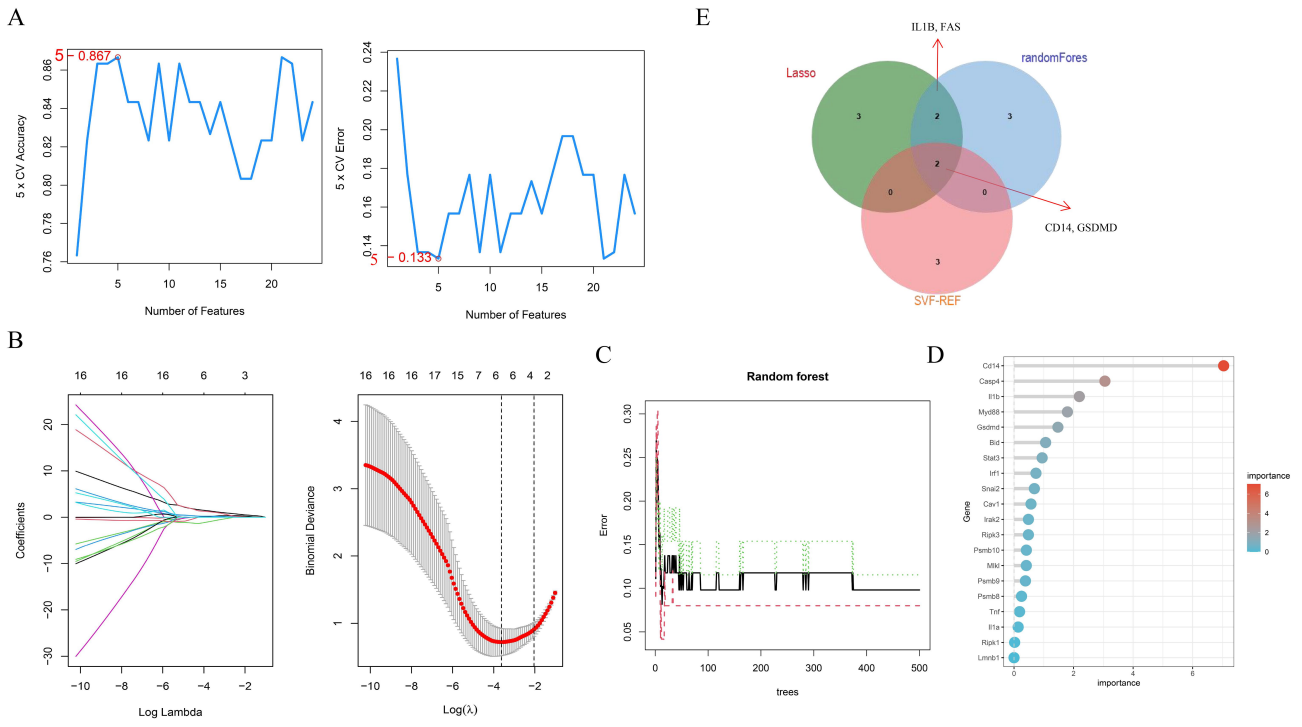

Figure 3 Signature genes selection. (**A**) The accuracy curve and error rate curve for 5-fold cross-validation based on SVM-RFE algorithm. (**B**) Lasso regression plot and 10-fold cross-validation plot. (**C**) RF error rate versus the number of classification trees. (**D**) The top 20 relatively significant genes based on RF algorithm. (**E**) Three algorithmic Venn diagram screening signature genes.

Table 3 The Results of Three Machine Learning Algorithms

	FeatureName	FeatureID	AvgRank		Gene	Coefficients		Gene	Importance
SVM-RFE	CD14	1	3.1	LASSO	(Intercept)	−20.52541387	RF	CD14	7.040699814
	GSDMD	10	5.4		CD14	1.303205256		CASP4	3.052567717
	DYNLL1	23	6.3		IL1β	8.58E-05		IL1β	2.193567885
	PSMB9	20	6.9		TNF	0.094865629		FAS	1.943585015
	STAT3	12	7.3		IRF1	0.199916584		MYD88	1.793590201
					GSDMD	1.130287863		GSDMD	1.473221718
					SNAI2	−0.85481821		BID	1.060887261
					FAS	0.232234042		STAT3	0.944497169
								IRF1	0.736430511
								SNAI2	0.682371795

Abbreviations: SVM-RFE, support vector machine-recursive signature elimination; LASSO, least absolute shrinkage and selection operator; RF, RandomForest; CD14, cluster of differentiation 14; GSDMD, Gasdermin D; DYNLL1, Dynein Light Chain LC8-Type 1; PSMB9, proteasome 20S subunit beta 9; STAT3, Signal transducer and activator of transcription 3; IL-1β, Interleukin—1β; TNF, tumor Necrosis Factor; IRF1, Interferon regulatory factor 1; SNAI2, Snail Family Transcriptional Repressor 2; FAS, factor-related Apoptosis; CASP4, caspase-4; MYD88, Myeloid differentiation factor 88; BID, BH3-Interacting Domain Death Agonist.

that the predicted probability of the model is fairly consistent with the actual probability, indicating that the model is quite accurate (Figure 4B). Additionally, ROC curve analysis can also be used to evaluate predictive correctness. The AUC of the ROC curve of nomogram and these signature genes was 0.957 of nomoscore, 0.932 of CD14, 0.823 of FAS, 0.791 of GSDMD, and 0.900 of IL1β respectively, implying that these signature genes had great diagnostic efficiency in the model (Figure 4C and D).

Immunological Infiltration Analysis

The results of ssGSEA scores of immune cells and immune functions between the control and SLI groups revealed that CD8+ T cells and B cells in the SLI group were lower than in the control group after excluding the items with not

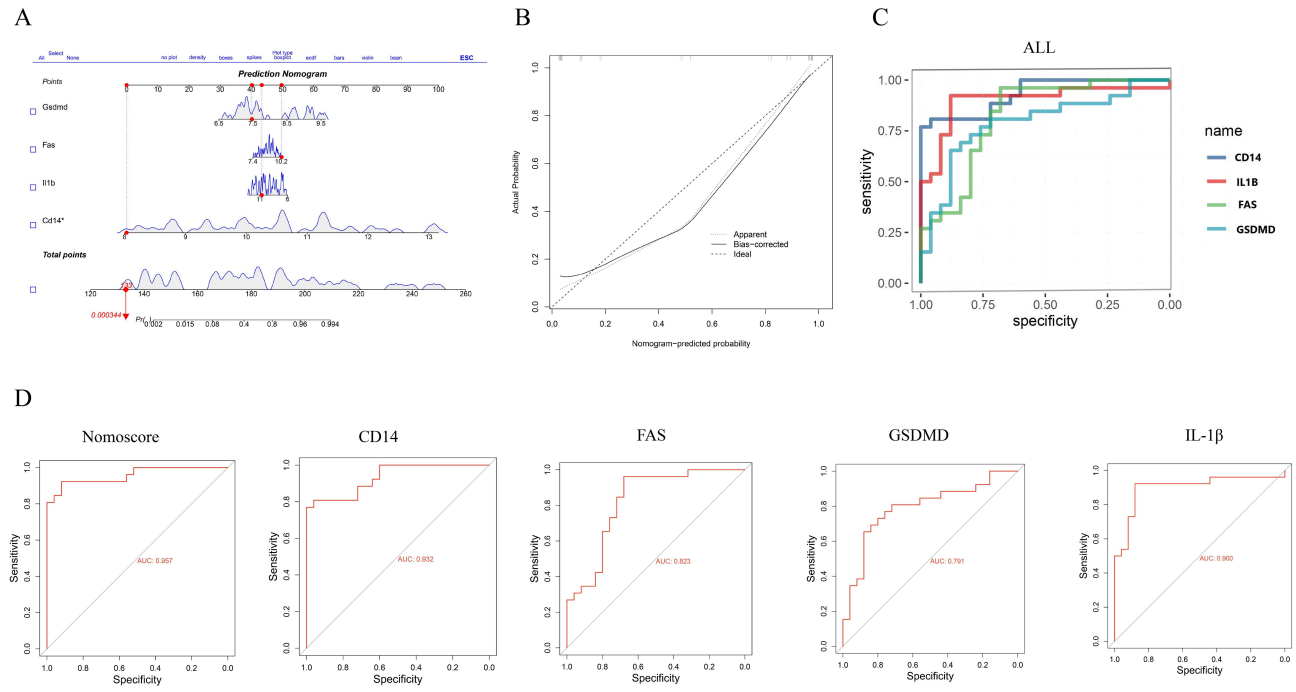

Figure 4 Construction and validation a diagnostic nomogram model. (**A**) A diagnostic nomogram was developed based on the four signature genes. (**B**) Calibration curves to assess the predictive power of the nomogram. (**C**) ROC curve of the four signature genes. (**D**) ROC curves of nomoscore and the four signature genes, respectively.

statistically significant ($p > 0.2$), and the rest immune cells and immune functions in the SLI group were higher than those in the control group ($p < 0.2$) (Figure 5A). The heat map of the correlation between signature genes and immunity showed that GSDMD was negatively correlated with mast cells, macrophages, CD8+ T cells and was positively correlated with others. After excluding entries that were not statistically significant, CD14, FAS, and IL1β were positively correlated with all remaining immune cells and immune functions (Figure 5B).

Correlation Analysis and the Expression Levels of the Signature Genes

Difference analysis was conducted to further determine the four signature genes expression levels between the control group and the SLI group, we found that these signature genes were highly expressed in SLI group based on difference expression analysis ($p < 0.05$) (Figure 6A–D). Furthermore, We performed the correlation analysis to better understand

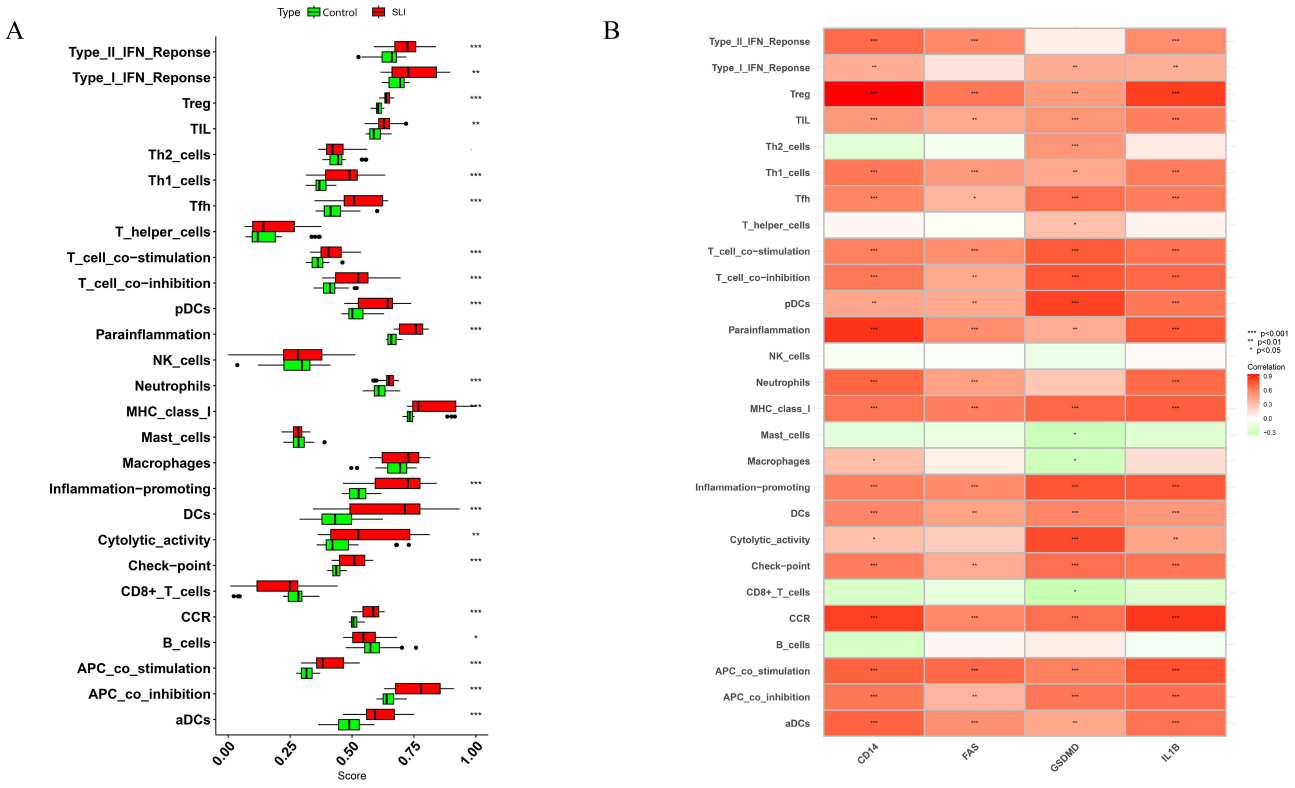

Figure 5 Correlation between SLI and immunity. (**A**) Comparison of ssGSEA scores of immune cells and immune functions between the SLI group and the control group. (**B**) Correlation between the characteristic genes and immunity. *p < 0.05, **p < 0.01, ***p < 0.001, "ns" represents no significance.

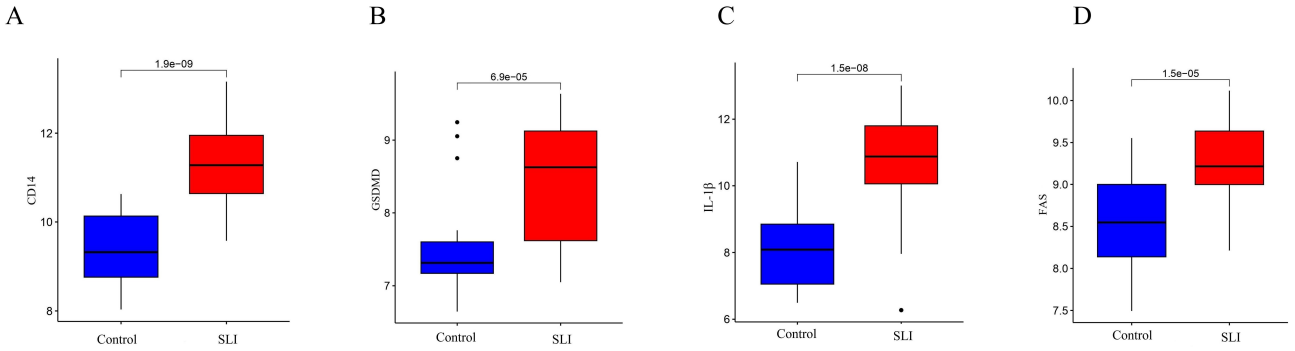

Figure 6 The expression levels of the four signature genes between the SLI group and the control group. (**A**) The expression level of CD14. (**B**) The expression level of GSDMD. (**C**) The expression level of IL-1β. (**D**) The expression level of FAS.

the correlation between the signature genes, the results of the heat map and the scatter plots of correlation coefficients indicated that FAS and CD14 (r = 0.75, p < 1e-0.5), CD14 and IL1β (r = 0.74, p < 1.4e-0.5), and FAS and IL1β (r = 0.7, p < 6.1e-0.5) were positively correlated, indicating that the signature genes CD14, FAS and IL1β may have had significantly similar features in SLI (Figure 7A–G).

H&E Staining

The lung sections of mice in the sham group showed normal alveolar structure, relatively homogeneous alveolar lumen volume, thin alveolar septum, no edema or inflammatory infiltrate, homogeneous cytoplasmic staining, clear nuclei. Whereas the lungs of the CLP group mice revealed alveolar congestion, inflammatory exudation, and thickening of the alveolar septum, with the higher lung injury score than the sham group (p < 0.0001) (Figure 8A and B).

Validation of Bioinformatics Results by qRT-PCR

The qRT-PCR results indicated that the mRNA expression levels CD14, FAS, and IL1β in lung tissues were significantly higher in the CLP group than the sham group (p < 0.05) and were consistent with the results of bioinformatics analysis (Figure 9A–C). However, the mRNA expression level of GSDMD was higher in the sham group than the CLP group (p > 0.05) (Figure 9D).

Discussion

Sepsis is a life-threatening organ dysfunction caused by a complex series of pathological processes resulting from a dysregulated host response to infection, often accompanied by a dysregulated immune response and multi-organ dysfunction, leading to high mortality rates and an enormous healthcare burden worldwide.[1,27] The lung is the most commonly affected organ, with approximately 50% of sepsis causing lung injury, but the exact mechanism remains unclear and effective drugs are extremely limited.[3,28,29] Recently, as the concept of PANoptosis was proposed, revealing the complex interplay of different cell death patterns in the development of disease, which has become a research hotspot

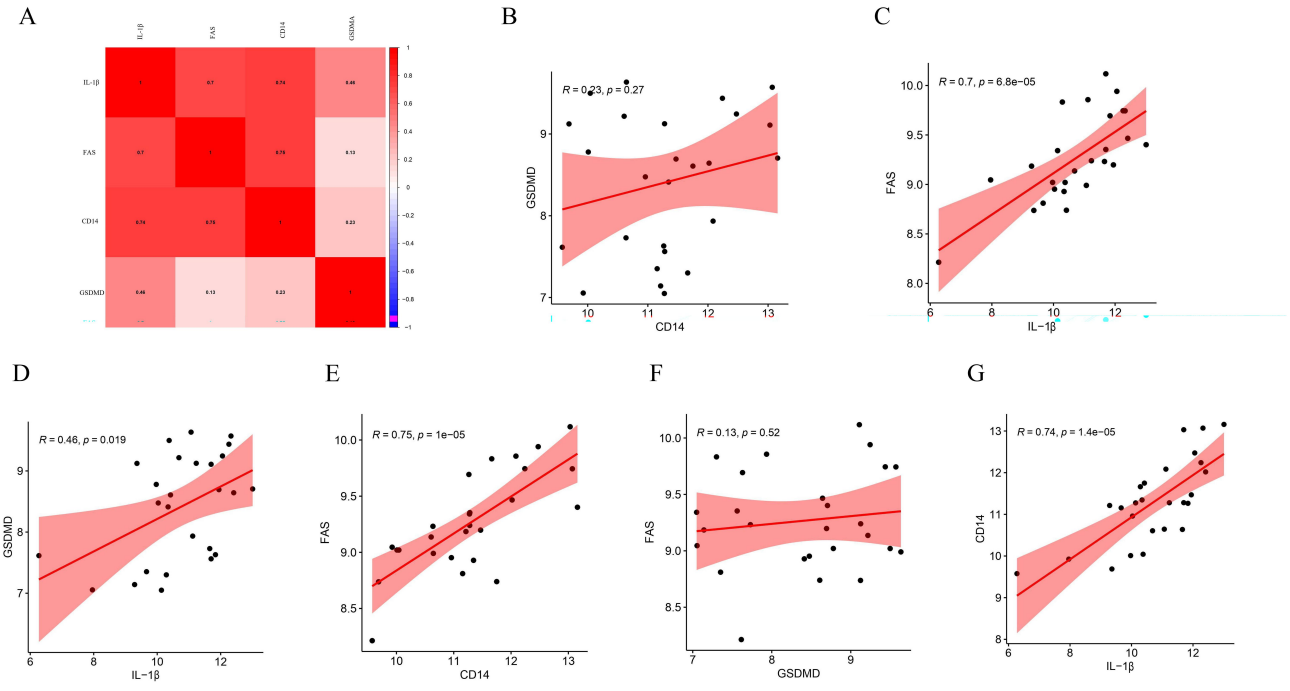

Figure 7 Correlation between the four signature genes. (**A**) Heat map of correlation. (**B**) A scatter plot between CD14 and GSDMD. (**C**) A scatter plot between IL-1β and FAS. (**D**) A scatter plot between IL-1β and GSDMD. (**E**) A scatter plot between CD14 and FAS. (**F**) A scatter plot between GSDMD and FAS. (**G**) A scatter plot between IL-1β and CD14.

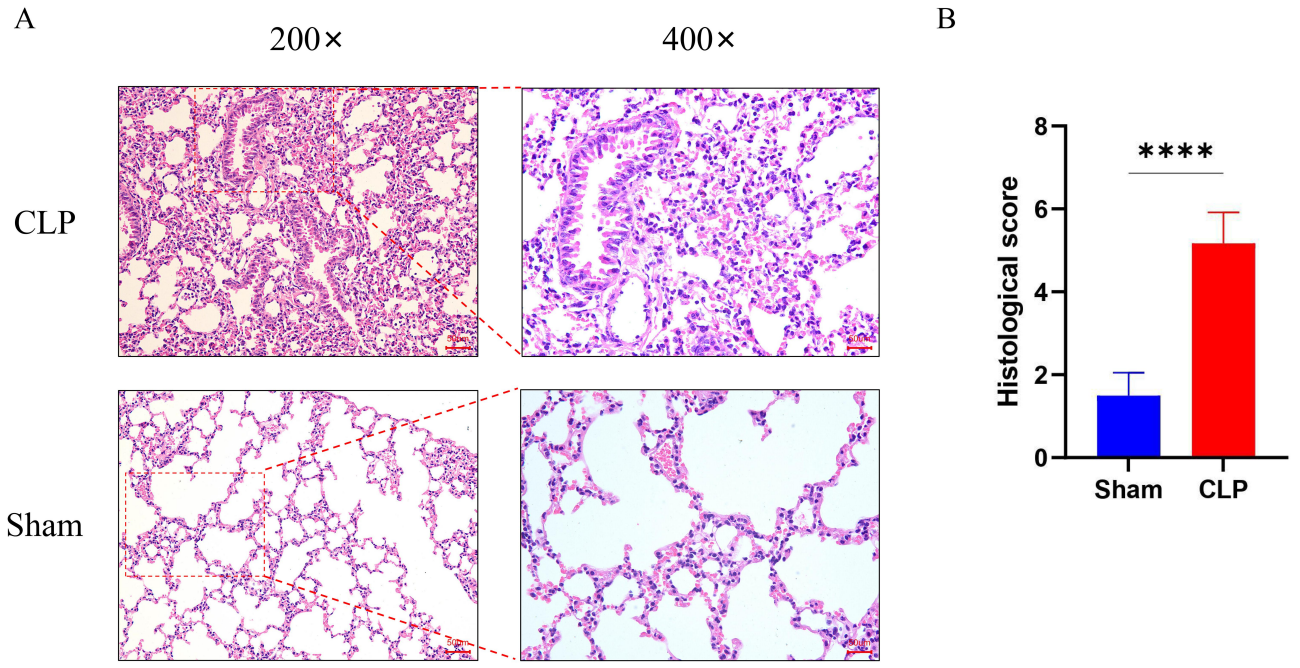

Figure 8 Lung pathological change of mice. (**A**) Results of H&E staining of the lung tissues (Images were magnified at 200× and 400×, Scale bar = 50 μm). (**B**) Lung injury score of HE staining (n=3). Data are represented as the mean ± SD. ****P < 0.0001.

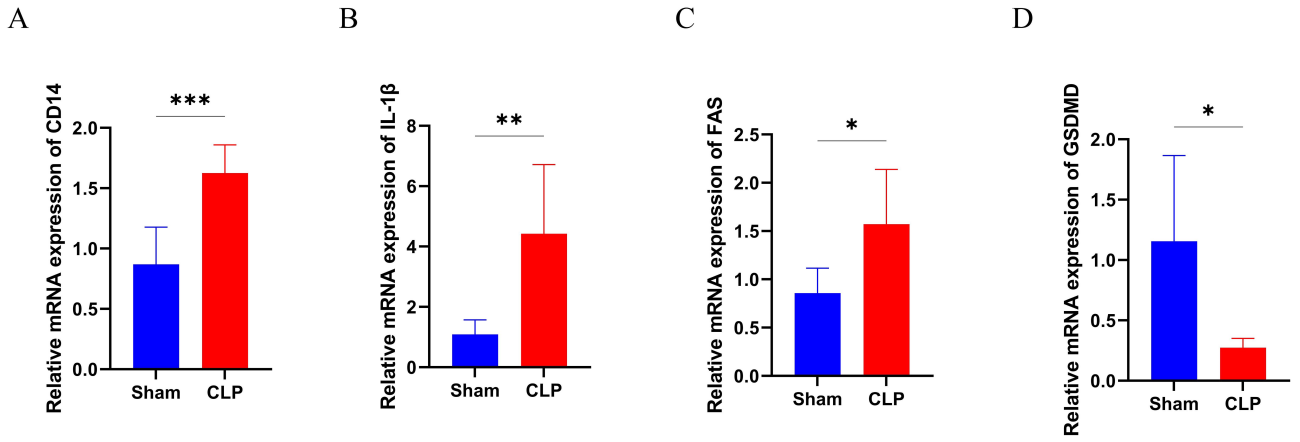

Figure 9 The results of RT-PCR experiment. (**A**–**D**) The mRNA expression levels of CD14, IL1β, FAS, and GSDMD in mice lung tissues (n=6). Data are represented as the mean ± SD. *P < 0.05, **P < 0.01, ***P < 0.001.

to identify new biomarkers and therapeutic targets.[30] However, the current research about the role of PANoptosis in SLI is insufficient.

With the rapid development of bioinformatics technologies and molecular studies, they play an important role in mechanistic research of related diseases and drug development. Our study utilized a thorough and in-depth assessment system to mine and validate the signature genes and molecular pathways of PANoptosis involved in SLI through bioinformatics. In particular, the use of machine learning algorithms and immune infiltration analysis makes the study more scientific and convincing, aiming to deeply explore the pathologic processes and molecular mechanisms of SLI and provide new ideas and therapeutic targets for research and clinical treatment.

In our study, we identified 675 DEGs and found 465 up-regulated genes and 210 down-regulated genes. The Volcano plot and heat map of DEGs revealed that multiple chemokines (CCL2, CCL3, CCL7, CCL12, and CCL17), CXC

chemokine subfamily (CXCL1, CXCL2, CXCL3, and CXCL10), interleukins (IL-6 and IL-1β), and Serum amyloid As (SAA1 and SAA3) were main up-regulated genes, Methyltransferase-like protein 7A2 (METTL7A2) was main down-regulated gene. Notably, the inflammatory hyperresponsive phase, macrophages polarize toward the M1 type and release large amounts of inflammatory factors (TNF-α, IL-6 and IL-1β) and chemokines in the early stages of sepsis. Moreover, chemokines are a class of small cellular factors or signaling proteins secreted by cells, and are also crucial active mediators in the immune response, which can induce the proliferation of immune cells to further participate in the immune response, activate a variety of enzyme activities and stimulate the killing activity of natural killer cells.[31] CXCL1 and CXCL2, as specific CXC chemokines, can effectively attract neutrophils and are important regulators of neutrophil infiltration in SLI.[32] In particular, it was found that inhibiting of CXCR2, the main receptor for CXCL2 and CXCL1, significantly alleviated the pulmonary accumulation of neutrophils in the sepsis mice.[33] As an acute-phase protein, SAA is highly expressed following infection and stress and can be used as a sensitive and reliable marker of inflammatory response for the early diagnosis of sepsis.[34,35] METTL7A is a member of the METTL family of methyltransferases, METTs can catalyze DNA methylation and are involved in inflammatory responses and immune dysregulation, and play an important role in lung cancer, pneumonia, and other diseases.[36]

By taking the intersection of 675 DEGs with 277 PANoptosis-related genes, 24 SPAN_DEGs were obtained. The results of PPI network presented that TNF, CASP1, IL-1β, Myd88, STAT3, and IRF1 were the top 6 genes in the network according to degree values. In the classical pyroptosis pathway, active caspase-1 (CASP1) can cleave GSDMD protein to form active N-terminus and C-terminus, and the N-terminus contributes to perforation of the cell membrane and cell death, and CASP1 can also process pro-IL-1β to form active IL-1β, which can be released into extracellular cells to amplify inflammation, whereas heat shock factor 1 (HSF1) can inhibit the activation of CASP1 and the maturation of IL-1β through the promotion of ubiquitination of NLRP3.[37] Myeloid differentiation factor 88 (MyD88) is an important junction protein molecule in the TLR4/MyD88/NF-κB signaling pathway, LPS-induced SLI was associated with activation of the TLR4/MyD88/NF-κB signaling pathway, which was significantly inhibited by Allicin, and down-regulated the expression of the inflammatory cytokines IL-1β, TNF-α, and IL-6.[38] STAT3 is a core member of the JAK/STAT signaling pathway, previous studies have shown that the JAK2/STAT3 signaling pathway can be activated by a number of cytokines in the early stage of sepsis, and aggravate SLI.[39] As a member of the interferon transcription factor family, interferon regulatory factor 1 (IRF1) is recognized as a key molecule in the regulation of macrophage M1 polarization and the development of sepsis-related ARDS, thereby promoting SLI.[40] These findings suggest that the core genes screened from SPAN_DEGs are closely related to multiple inflammatory pathways and all of them are key genes on the pathways. Therefore, it can be reasonably inferred that PANoptosis may participate in the complex immuno-inflammatory regulatory process in the pathogenesis of SLI.

Subsequently, GO, KEGG and GSEA enrichment analysis showed that SPAN_DEGs mainly associated with TNF-signaling pathway, NOD-like receptor (NODs) signaling pathway, cytosolic DNA-sensing pathway, Toll-like receptor (TLRs) signaling pathway, NF-κB signaling pathway, IL-17 signaling pathway. These regulatory pathways have been reported to be closely associated with SLI in previous studies. TNF is one of the cytokines that make up the acute-phase response and is involved in the systemic inflammatory response, triggering the activation of a number of pathways, including the NF-κB and MAPK pathways. In addition, TNF-α has also been found to participate in sepsis immuno-suppression by increasing apoptosis, and its plasma level is significantly correlated with sepsis mortality.[41,42] During lung injury, macrophages recognize pathogen-associated molecular patterns (PAMPs) of microorganisms or danger-associated molecular patterns (DAMPs) through TLRs, NODs, and a variety of other pattern-recognition receptors, and then clear and phagocytose them. In addition, pattern recognition leads to the release of cytokines involved in the initial response, TNF-α, type I IFN, and IL-1β, which are released and will activate lung macrophages through the NF-κβ or IRF signaling pathways.[43,44] A research focused on bioinformatics analysis and experimental verification revealed that IL-17 signaling pathway is significantly associated with the development of pneumonia-induced sepsis, and activation of the IL-17 signaling pathway promotes cellular charring in pneumonia-induced sepsis.[45] These findings suggested that the pro-inflammatory role of SPAN_DEGs in SLI may be exerted by modulating the above pathways.

Using SVM-RFE, LASSO logistic regression analysis, and RF machine learning algorithm, we screened four signature genes CD14, GSDMD, IL1β, and FAS, which are strongly associated with PANoptosis in SLI and have

significant diagnostic value. Besides, we found the four signature genes were highly expressed in the SLI group and there was a positive correlation between them. CD14, a member of the cell surface glycoprotein family, is a high-affinity receptor that ensures that TLR4 responds to LPS, as well as being important for the production of pro-inflammatory cytokines by macrophages.[46] Extracellular CD14 is important for host defense during infection, particularly for bacterial clearance.[47] Additionally, a study also found that CD14 is a plasma membrane-associated protein that is part of the P2X7 receptor secretome, and its deficiency impairs macrophage pro-inflammatory cytokines production.[46] As a member of the gasdermin family, GSDMD is the ultimate effector protein of cellular death, and it can mediate organ damage, cellular regulation, and molecular mediation in the development of sepsis.[48] Experimental studies have found that in the LPS-induced sepsis mouse model, the symptoms of the GSDMD knockout mice were significantly reduced, and the survival rate was greatly increased,[49] suggesting that pyroptosis plays a key role in sepsis, whereas GSDMD can serve as an important target gene. As a core factor in sepsis-induced inflammatory response and tissue injury, IL-1β produced by pro-inflammatory macrophages is also involved in cytokine storm-induced pulmonary vascular leakage inducing inflammatory injury in sepsis.[50] Meanwhile, IL-1β is involved in the cAMP-CREB-VE-calmodulin pathway, and down-regulation of this pathway is a crucial mechanism for lung endothelial barrier damage and further lung injury in the pathogenesis of sepsis.[51] Noticeably, we found some Chinese herbal medicine compounds or monomers could alleviate SLI by modulating apoptosis, pyroptosis, or necrosis. For example, Salidroside pretreatment was found to alleviate $PM_{2.5}$-induced lung injury via inhibition of apoptosis and pyroptosis through regulating NLRP3 inflammasome pathway.[52] A CLP-induced SLI mouse model was constructed to confirm the effect of CD14, GSDMD, IL1β, and FAS on SLI. The results of qRT-PCR consistently showed that CD14, IL1β, and FAS expression was significantly increased in SLI, only the expression of GSDMD was not inconsistent with our bioinformatics analysis.

We further evaluated the immune cell infiltration between the two groups. Unsurprisingly, the SLI group had significantly higher levels of most types of immune cell infiltration, except for CD8+ T cells and B cells. It is well known that the pathogenesis of sepsis involves aberrant activation of immune cells in the early stages and sepsis-associated immunosuppression, which leads to apoptosis and a decrease in the number of CD8+ T cells.[53] B cells act as a major player in acquired immunity, it was reported that B cells were found to be severely reduced in the bone marrow and spleen of SARS-CoV-2 infected decedents, and this impeded the humoral immune response to SARS-CoV-2 infection.[54] Besides, our research found that CD14, FAS, and IL1β are tightly associated with a variety of immune cells and immune functions, indicating that these signature genes may be involved in regulating the immune-inflammatory response during PANoptosis in SLI.

Nevertheless, some limitations do exist in our study. Firstly, the sample size included was insufficient, in addition, there was some heterogeneity in different datasets, which could cause some bias in our results. To address this, the sample size needs to be expanded later to further validate the results and establish a more accurate clinical model. Secondly, our study lacked clinical samples for validation, in order to solve this problem, further in-depth clinical studies can be followed. Finally, the mechanism by which these signature genes affect SLI by regulating pan-apoptosis needs to be further investigated. It is important to recognize that our study provides valuable insights for the diagnosis and treatment of SLI by targeting PANoptosis.

Conclusions

In conclusion, our study deeply explored the relationship between PANoptosis process and SLI through comprehensive bioinformatics analysis, and finally identified four characteristic genes, CD14, GSDMD, IL-1β, and FAS, respectively. Then, these signature genes were highly correlated with immune cell infiltration and immunological response and consistently associated with multiple Immunoinflammatory pathways, indicating that they may contribute to SLI by regulating immune processes during PANoptosis. Finally, we found that CD14, FAS, and IL-1β may be involved in PANoptosis to drive the progression of SLI by experimental verification. This study will contribute to the development of early diagnostic indicators and immunotherapy methods for SLI.

Abbreviations

SLI, sepsis-induced lung injury; GEO, Gene Expression Omnibus; DEGs, Differentially expressed genes; SPAN_DEGs, DEGs related to PANoptosis; PPI, Protein–Protein Interaction; H&E, hematoxylineosin; qRT-PCR, quantitative real-time PCR; NODs, NOD-like receptor; TLRs, Toll-like receptor; CLP, cecum ligation and puncture; ALI, acute lung injury; ARDS, acute respiratory distress syndrome; TNFR1, TNF receptor 1; caspase, cysteinyl aspartate-specific proteinase; NLRP3, NOD-like receptor thermal protein domain associated protein 3; ASC, apoptosis-associated speck-like protein containing a CARD; GSDMD, Gasdermin D; RIPK1, receptor-interacting protein kinase 1; MLKL, mixed-lineage kinase domain-like; ZBP1, Z-DNA binding protein 1; APN, Aminopeptidase N; SVM-RFE, support vector machine-recursive signature elimination; LASSO, least absolute shrinkage and selection operator; RF, RandomForest; ROC, receiver operating characteristic; SVA, surrogate variable analysis; FC, fold-change; KEGG, Kyoto Encyclopedia of Genes and Genomes; GO, gene ontology; CC, cellular components; MF, molecular functions; BP, biological pathways; GSEA, Gene Set Enrichment Analysis; aDCs, activated dendritic cells; iDCs, immature DCs; NK cells, natural killer cells; pDCs, plasmacytoid DCs; Tfh, T follicular helper; Th1 cells, T helper type 1; TIL, tumor-infiltrating lymphocytes; APC, antigen presenting cell; CCR, chemokine C-C-Motif receptor; HLA, human leukocyte antigen; MHC, major histocompatibility complex; IFN, interferon; SPF, specific pathogen-free; CARD, caspase recruitment domain; NF-κB, nuclear factor kappa B; METTL7A2, Methyltransferase-like protein 7A2; HSF1, heat shock factor 1; MyD88, Myeloid differentiation factor 88; IRF1, interferon regulatory factor 1; PAMPs, pathogen-associated molecular patterns; DAMPs, danger-associated molecular patterns.

Data Sharing Statement

The original data of the study are appended to the article/Supplementary Material. Further inquiries can be addressed directly to the corresponding author.

Ethics Statement

The study involving human data was approved by the Ethics Committee of Foshan Hospital of Traditional Chinese Medicine (KY020231009). Besides, our research was conducted according to the International Ethics Guidelines and the National Institutes of Health Guidelines Concerning the Care and Use of Laboratory Animals. The animal study was approved by the Laboratory Animal Welfare and Ethics Committee, School of Pharmaceutical Sciences, Guangzhou University of Chinese Medicine (No. ZYD-2023-102).

Acknowledgments

We thank the researchers of GSE15379, GSE23767, GSE52474, and GSE60088 for sharing data online.

Author Contributions

All authors made a significant contribution to the work reported, whether that is in the conception, study design, execution, acquisition of data, analysis and interpretation, or in all these areas; took part in drafting, revising or critically reviewing the article; gave final approval of the version to be published; have agreed on the journal to which the article has been submitted; and agree to be accountable for all aspects of the work.

Funding

The study was supported by the National Natural Science Foundation of China (Grant number 82374216).

Disclosure

The authors declare there are no competing interests in this work.

References

1. Evans L, Rhodes A, Alhazzani W, et al. Executive summary: surviving sepsis campaign: international guidelines for the management of sepsis and septic shock 2021. *Crit Care Med*. 2021;49(11):1974–1982. doi:10.1097/CCM.0000000000005357
2. Sadowitz B, Roy S, Gatto LA, Habashi N, Nieman G. Lung injury induced by sepsis: lessons learned from large animal models and future directions for treatment. *Expert Rev Anti Infect Ther*. 2011;9(12):1169–1178. doi:10.1586/eri.11.141
3. Sevransky JE, Levy MM, Marini JJ. Mechanical ventilation in sepsis-induced acute lung injury/acute respiratory distress syndrome: an evidence-based review. *Crit Care Med*. 2004;32(11 Suppl):S548–S553. doi:10.1097/01.CCM.0000145947.19077.25
4. Sessler CN, Bloomfield GL, Fowler AR. Current concepts of sepsis and acute lung injury. *Clin Chest Med*. 1996;17(2):213–235. doi:10.1016/S0272-5231(05)70310-5
5. Chen R, Cao C, Liu H, et al. Macrophage Sprouty4 deficiency diminishes sepsis-induced acute lung injury in mice. *Redox Biol*. 2022;58:102513. doi:10.1016/j.redox.2022.102513
6. Kim WY, Hong SB. Sepsis and acute respiratory distress syndrome: recent update. *Tuberc Respir Dis*. 2016;79(2):53–57. doi:10.4046/trd.2016.79.2.53
7. Wang Y, Kanneganti TD. From pyroptosis, apoptosis and necroptosis to PANoptosis: a mechanistic compendium of programmed cell death pathways. *Comput Struct Biotechnol J*. 2021;19:4641–4657. doi:10.1016/j.csbj.2021.07.038
8. Place DE, Lee S, Kanneganti TD. PANoptosis in microbial infection. *Curr Opin Microbiol*. 2021;59:42–49. doi:10.1016/j.mib.2020.07.012
9. Pandian N, Kanneganti TD. PANoptosis: a unique innate immune inflammatory cell death modality. *J Immunol*. 2022;209(9):1625–1633. doi:10.4049/jimmunol.2200508
10. Cui Y, Wang X, Lin F, et al. MiR-29a-3p improves acute lung injury by reducing alveolar epithelial cell PANoptosis. *Aging Dis*. 2022;13(3):899–909. doi:10.14336/AD.2021.1023
11. Chan FK, Luz NF, Moriwaki K. Programmed necrosis in the cross talk of cell death and inflammation. *Annu Rev Immunol*. 2015;33:79–106. doi:10.1146/annurev-immunol-032414-112248
12. Gong T, Zhang X, Peng Z, et al. Macrophage-derived exosomal aminopeptidase N aggravates sepsis-induced acute lung injury by regulating necroptosis of lung epithelial cell. *Commun Biol*. 2022;5(1):543. doi:10.1038/s42003-022-03481-y
13. Kumar N, Narayan DN, Gupta D, Gupta K, Bindra J, Gritli H. Efficient automated disease diagnosis using machine learning models. *J Healthc Eng*. 2021;2021:9983652. doi:10.1155/2021/9983652
14. Zhou Y, Shi W, Zhao D, Xiao S, Wang K, Wang J. Identification of immune-associated genes in diagnosing aortic valve calcification with metabolic syndrome by integrated bioinformatics analysis and machine learning. *Front Immunol*. 2022;13:937886. doi:10.3389/fimmu.2022.937886
15. Barrett T, Wilhite SE, Ledoux P, et al. NCBI GEO: archive for functional genomics data sets--update. *Nucleic Acids Res*. 2013;41(Database issue):D991–D995. doi:10.1093/nar/gks1193
16. Song F, Wang CG, Mao JZ, et al. PANoptosis-based molecular subtyping and HPAN-index predicts therapeutic response and survival in hepatocellular carcinoma. *Front Immunol*. 2023;14:1197152. doi:10.3389/fimmu.2023.1197152
17. Walter W, Sanchez-Cabo F, Ricote M. GOplot: an R package for visually combining expression data with functional analysis. *Bioinformatics*. 2015;31(17):2912–2914. doi:10.1093/bioinformatics/btv300
18. Subramanian A, Tamayo P, Mootha VK, et al. Gene set enrichment analysis: a knowledge-based approach for interpreting genome-wide expression profiles. *Proc Natl Acad Sci U S A*. 2005;102(43):15545–15550. doi:10.1073/pnas.0506580102
19. Sanz H, Valim C, Vegas E, Oller JM, Reverter F. SVM-RFE: selection and visualization of the most relevant features through non-linear kernels. *BMC Bioinf*. 2018;19(1):432. doi:10.1186/s12859-018-2451-4
20. Engebretsen S, Bohlin J. Statistical predictions with glmnet. *Clin Clin Epigenet*. 2019;11(1):123. doi:10.1186/s13148-019-0730-1
21. Ishwaran H, Kogalur UB. Consistency of random survival forests. *Stat Probab Lett*. 2010;80(13–14):1056–1064. doi:10.1016/j.spl.2010.02.020
22. Pan X, Jin X, Wang J, Hu Q, Dai B. Placenta inflammation is closely associated with gestational diabetes mellitus. *Am J Transl Res*. 2021;13(5):4068–4079.
23. Xing Y, Tian Z, Jiang Y, et al. A practical nomogram based on systemic inflammatory markers for predicting portal vein thrombosis in patients with liver cirrhosis. *Ann Med*. 2022;54(1):302–309. doi:10.1080/07853890.2022.2028893
24. Mandrekar JN. Receiver operating characteristic curve in diagnostic test assessment. *J Thorac Oncol*. 2010;5(9):1315–1316. doi:10.1097/JTO.0b013e3181ec173d
25. Rittirsch D, Huber-Lang MS, Flierl MA, Ward PA. Immunodesign of experimental sepsis by cecal ligation and puncture. *Nat Protoc*. 2009;4(1):31–36. doi:10.1038/nprot.2008.214
26. Shen W, Gan J, Xu S, Jiang G, Wu H. Penehyclidine hydrochloride attenuates LPS-induced acute lung injury involvement of NF-kappaB pathway. *Pharmacol Res*. 2009;60(4):296–302. doi:10.1016/j.phrs.2009.04.007
27. Singer M, Deutschman CS, Seymour CW, et al. The third international consensus definitions for sepsis and septic shock (sepsis-3). *JAMA*. 2016;315(8):801–810. doi:10.1001/jama.2016.0287
28. Martin GS, Mannino DM, Eaton S, Moss M. The epidemiology of sepsis in the United States from 1979 through 2000. *N Engl J Med*. 2003;348(16):1546–1554. doi:10.1056/NEJMoa022139
29. Patel VJ, Biswas RS, Mehta HJ, Joo M, Sadikot RT. Alternative and natural therapies for acute lung injury and acute respiratory distress syndrome. *Biomed Res Int*. 2018;2018:2476824. doi:10.1155/2018/2476824
30. Wu H, Wang T, Liu Y, et al. Mitophagy promotes sorafenib resistance through hypoxia-inducible ATAD3A dependent axis. *J Exp Clin Cancer Res*. 2020;39(1):274. doi:10.1186/s13046-020-01768-8
31. Hwaiz R, Hasan Z, Rahman M, et al. Rac1 signaling regulates sepsis-induced pathologic inflammation in the lung via attenuation of Mac-1 expression and CXC chemokine formation. *J Surg Res*. 2013;183(2):798–807. doi:10.1016/j.jss.2013.02.045
32. Ding Z, Du F, Averitt VR, et al. Targeting S100A9 reduces neutrophil recruitment, inflammation and lung damage in abdominal sepsis. *Int J Mol Sci*. 2021;22(23). doi:10.3390/ijms222312923
33. Zhang S, Rahman M, Zhang S, Qi Z, Thorlacius H. Simvastatin antagonizes CD40L secretion, CXC chemokine formation, and pulmonary infiltration of neutrophils in abdominal sepsis. *J Leukoc Biol*. 2011;89(5):735–742. doi:10.1189/jlb.0510279

34. Xiao Y, Ren C, Chen G, et al. Neutrophil membrane-mimicking nanodecoys with intrinsic anti-inflammatory properties alleviate sepsis-induced acute liver injury and lethality in a mouse endotoxemia model. *Mater Today Bio*. 2022;14:100244. doi:10.1016/j.mtbio.2022.100244
35. Balayan S, Chauhan N, Chandra R, Jain U. Molecular imprinting based electrochemical biosensor for identification of serum amyloid A (SAA), a neonatal sepsis biomarker. *Int J Biol Macromol*. 2022;195:589–597. doi:10.1016/j.ijbiomac.2021.12.045
36. Huang X, Kong G, Li Y, et al. Decitabine and 5-azacitidine both alleviate LPS induced ARDS through anti-inflammatory/antioxidant activity and protection of glycocalyx and inhibition of MAPK pathways in mice. *Biomed Pharmacother*. 2016;84:447–453. doi:10.1016/j.biopha.2016.09.072
37. Shi X, Li T, Liu Y, et al. HSF1 protects sepsis-induced acute lung injury by inhibiting NLRP3 inflammasome activation. *Front Immunol*. 2022;13:781003. doi:10.3389/fimmu.2022.781003
38. Shen N, Cheng A, Qiu M, Zang G. Allicin improves lung injury induced by sepsis via regulation of the Toll-Like Receptor 4 (TLR4)/Myeloid Differentiation Primary Response 88 (MYD88)/Nuclear Factor kappa B (NF-kappaB) pathway. *Med Sci Monit*. 2019;25:2567–2576. doi:10.12659/MSM.914114
39. Wang F, Wang M, Wang J, et al. Maresin1 ameliorates sepsis-associated lung injury by inhibiting the activation of the JAK2/STAT3 and MAPK/NF-kappaB signaling pathways. *Microb Pathog*. 2020;148:104468. doi:10.1016/j.micpath.2020.104468
40. Wang A, Kang X, Wang J, Zhang S. IFIH1/IRF1/STAT1 promotes sepsis associated inflammatory lung injury via activating macrophage M1 polarization. *Int Immunopharmacol*. 2023;114:109478. doi:10.1016/j.intimp.2022.109478
41. He J, Zhang Q, Zhang W, et al. The interleukin-27 −964A>G polymorphism enhances sepsis-induced inflammatory responses and confers susceptibility to the development of sepsis. *Crit Care*. 2018;22(1):248. doi:10.1186/s13054-018-2180-0
42. Zhang M, Zhao Y, Liu Q. Tumor necrosis factor-alpha −308G/A and −238G/A polymorphisms are associated with increased risks of sepsis: evidence from an updated meta-analysis. *Apmis*. 2017;125(5):459–467. doi:10.1111/apm.12661
43. Yujie HE, Jianping P. 病原菌对 NOD 样受体及 Toll 样受体信号通路□□ 介导的固有免疫逃逸机制研究进展 [Progress on mechanisms for pathogens to evade NOD-like receptor and Toll-like receptor signaling pathways]. *Zhejiang Da Xue Xue Bao Yi Xue Ban*. 2017;46(2):218–224. Chinese. doi:10.3785/j.issn.1008-9292.2017.04.16
44. Cassetta L, Cassol E, Poli G. Macrophage polarization in health and disease. *ScientificWorldJournal*. 2011;11:2391–2402. doi:10.1100/2011/213962
45. Li LL, Dai B, Sun YH, Zhang TT. The activation of IL-17 signaling pathway promotes pyroptosis in pneumonia-induced sepsis. *Ann Transl Med*. 2020;8(11):674. doi:10.21037/atm-19-1739
46. Alarcon-Vila C, Baroja-Mazo A, de Torre-Minguela C, et al. CD14 release induced by P2X7 receptor restricts inflammation and increases survival during sepsis. *Elife*. 2020;9. doi:10.7554/eLife.60849
47. Qin K, Ma S, Li H, et al. GRP78 impairs production of lipopolysaccharide-induced cytokines by interaction with CD14. *Front Immunol*. 2017;8:579. doi:10.3389/fimmu.2017.00579
48. Shao R, Lou X, Xue J, Ning D, Chen G, Jiang L. Review: the role of GSDMD in sepsis. *Inflamm Res*. 2022;71(10–11):1191–1202. doi:10.1007/s00011-022-01624-9
49. Shi J, Zhao Y, Wang K, et al. Cleavage of GSDMD by inflammatory caspases determines pyroptotic cell death. *Nature*. 2015;526(7575):660–665. doi:10.1038/nature15514
50. London NR, Zhu W, Bozza FA, et al. Targeting Robo4-dependent Slit signaling to survive the cytokine storm in sepsis and influenza. *Sci Transl Med*. 2010;2(23):19r–23r. doi:10.1126/scitranslmed.3000678
51. Xiong S, Hong Z, Huang LS, et al. IL-1beta suppression of VE-cadherin transcription underlies sepsis-induced inflammatory lung injury. *J Clin Invest*. 2020;130(7):3684–3698. doi:10.1172/JCI136908
52. Shi S, Huang D, Wu Y, et al. Salidroside pretreatment alleviates PM(2.5) caused lung injury via inhibition of apoptosis and pyroptosis through regulating NLRP3 inflammasome. *Food Chem Toxicol*. 2023;177:113858. doi:10.1016/j.fct.2023.113858
53. Yuan Y, Hua L, Zhou J, et al. The effect of artesunate to reverse CLP-induced sepsis immunosuppression mice with secondary infection is tightly related to reducing the apoptosis of T cells via decreasing the inhibiting receptors and activating MAPK/ERK pathway. *Int Immunopharmacol*. 2023;124(Pt A):110917. doi:10.1016/j.intimp.2023.110917
54. Ihlow J, Michaelis E, Greuel S, et al. B cell depletion and signs of sepsis-acquired immunodeficiency in bone marrow and spleen of COVID-19 deceased. *Int J Infect Dis*. 2021;103:628–635. doi:10.1016/j.ijid.2020.12.078